Observational evidence of particle hygroscopic growth in the UTLS over the Tibetan Plateau

Qianshan He[1,2], Jianzhong Ma[3], Xiangdong Zheng[3], Xiaolu Yan[3], Holger Vömel[4], Frank G. Wienhold[5], Wei Gao[1,2], Dongwei Liu[1,2], Guangming Shi[6],Tiantao Cheng[7]

[1]Shanghai Meteorological Service, Shanghai, China
[2]Shanghai Key Laboratory of Meteorology and Health, Shanghai, China
[3]State Key Laboratory of Severe Weather & CMA Key Laboratory of Atmospheric Chemistry, Chinese Academy of Meteorological Sciences, Beijing, China
[4]Earth Observing Laboratory, National Center for Atmospheric Research, Boulder, CO, USA
[5]ETH Zurich,Institute for Atmospheric and Climate Science (IAC),CH-8092 Zurich,Switzerland.
[6]Chongqing Institute of Green and Intelligent Technology, Chinese Academy of Sciences, Chongqing, China
[7]Department of Atmospheric and Oceanic Sciences, Institute of Atmospheric Sciences, Fudan University, Shanghai, China

Correspondence to: Jianzhong Ma (majz@cma.gov.cn)

Key Points:

1. Balloon-borne measurements show an enhanced aerosol layer consisting dominantly of fine particles in the UTLS over the Tibetan Plateau.

2.Water vapor is important in determining the size, and therefore radiative properties, of the particles.

Abstract

We measured the vertical profiles of backscatter ratio (BSR) using the balloon-borne, lightweight Compact Optical Backscatter AerosoL Detector (COBALD) instruments above Linzhi, located in the southeastern Tibetan Plateau, in the summer of 2014. An enhanced aerosol layer in the upper troposphere/lower stratosphere (UTLS), with BSR (455 nm)>1.1 and BSR (940 nm)>1.4, was observed. The Color Index (CI)

of the enhanced aerosol layer, defined as the ratio of aerosol backscatter ratios (ABSR) at wavelengths of 940 nm and 455 nm, varied from 4 to 8, indicating the prevalence of fine particles with mode radius less than 0.1 μm. We find that except for the very small particles (mode radius smaller than 0.04 μm) at low relative humidity (RHi < 40%), the relatively large particles in the aerosol layer were generally very hydrophilic as their size increased dramatically with relative humidity. This result indicates that water vapor can play a very important role in increasing the size of fine particles in the UTLS over the Tibetan Plateau. Our observations provide observation-based evidence supporting that aerosol particle   hygroscopic growth is an important factor influencing the radiative properties of the Asian Tropopause Aerosol Layer (ATAL) during the Asian summer monsoon.

Keywords: ATAL, hygroscopic growth, COBALD, Tibetan Plateau

1. Introduction

The Asian Tropopause Aerosol Layer (ATAL) extends over a large area within the Asian summer monsoon circulation and may significantly influence ozone, cirrus clouds and global climate by chemical, micro-physical and radiative processes [Gettelman et al., 2011; Vernier et al., 2011; Fadnavis et al., 2013; Thomason and Vernier, 2013; Vernier et al., 2015]. Particles in the ATAL are likely to be lifted to the lower stratosphere by the large-scale upward circulation within the south Asian anticyclone [Park et al., 2007], and then influence the aerosol amount in the global stratosphere significantly. Solomon et al. [2011] found that the radiative forcing of increased aerosols in the global stratosphere from 2000 to 2010 is $-0.1 \mathrm{W} \cdot \mathrm{m}^{-2}$, which weakened the global warming effect from increasing greenhouse gas concentrations.In addition to the elevated concentration of aerosols found in the ATAL as mentioned above, the concentrations of tropospheric trace gases (i.e., water vapor, CO, CH_4 and HCN) are higher within the Asian summer monsoon anticyclone than in surrounding regions, while the stratospheric trace gases (i.e, O_3, HNO_3 and HCl) are lower [Park et al., 2004; Randel et al., 2010]. Actually, the elevated aerosol concentration near the

tropopause over the Tibetan Plateau has also been observed by lidar and balloon borne measurements [Kim et al., 2003; Tobo et al., 2007; He et al., 2014]. Li [2005] showed that the aerosol plume is detectable in the anticyclone around the altitude of 150 hPa over the Tibetan Plateau through satellite observations and model study.

Sources and formation mechanism of aerosols in the UTLS, especially over the tropics, have been studied over the past decades. New particle formation events can occur at very low temperatures accompanied by the outflow of convective systems, as observed in the West African Monsoon [Frey et al., 2011].. Both condensation and coagulation contribute to the particle growth, even though these two processes are triggered by different mechanisms. Model studies have shown that coagulation is more important than nucleation in the control of the number concentration of fine particles (with diameter larger than 10 nm) in the UTLS [English et al., 2011; Pierce and Adams, 2009; Timmreck et al., 2010]. Compared with coagulation, the effect of condensation on particle growth is less documented in previous studies. Weigel et al. [2011] found that supersaturated gases, which can nucleate to form neutral and charged molecular clusters, also condense onto pre-existing aerosol particles. Earlier studies focusing on polar stratospheric clouds (PSCs) over the winter poles demonstrated that stratospheric aqueous H_2SO_4 aerosol can absorb a large amount of gaseous HNO_3 and H_2O at temperatures (about 200K) between the nitric acid trihydrate (NAT) and ice frost points [Carslaw et al., 1994; Tabazadeh et al., 1994], leading to a steep increase in particle volume.. These aerosols and PSCs are composed either of supercooled ternary solution (STS) droplets ($HNO_3 \cdot H_2O \cdot H_2SO_4$), ice particles or solid hydrates (most likely NAT) and can grow to larger particles that are easy to sediment [Voigt et al., 2008; Engel, 2013]. However, unlike the studies about PSCs, the growth mechanism of the particles in the ATAL is still vague due to the lack of sufficient observations.

In-depth investigations on the aerosol size distribution, chemical composition and growth process are needed for a better understanding of the characteristics and formation mechanism of ATAL. It is difficult to obtain much more information merely by means of remote sensing measurements, such as satellite and lidar, because those sensors are not sensitive to ultra-fine particles. In such case, balloon and/or air borne *in*

situ measurement provide an additional and even better tool for exploring the ATAL. Using a balloon-borne optical particle counter at Lhasa, China, Tobo et al. (2007) measured the vertical profiles of aerosols and found occurrences of relatively high number concentrations of sub-micron size aerosols near the tropopause region during the Asian summer monsoon period. They considered that the enhanced aerosol layer in the UTLS connected closely with the transportation of water vapor from the Asian summer monsoon. An increased amount of water vapor was found in the UTLS within the Asian summer monsoon anticyclone (Bian et al., 2012; Li et al., 2017). A series of balloon borne activities between 2014 and 2017 over India and Saudi Arabia during the Balloon Measurements of the Asian Tropopause Aerosol Layer (BATAL) campaigns revealed that the ATAL is composed of mostly small (r < 0.25 μm) liquid (~80%–95%) aerosols with the dominant composition of nitrate (Vernier et al., 2017). New particle formation and growth of particles by accretion of additional low volatility materials (e.g., H_2SO_4) tend to be an irreversible but slow progress due to limited amount of condensable gases, In contrast, hygroscopic growth of particles is a dynamic and typically reversible process, and may affect the size of particles and its variation in the ATAL more remarkably in a relatively short time since sufficient amount of water vapor can be frequently lofted to the UTLS via deep convection during the Asian monsoon [Fu et al., 2006].

As part of the project Tibetan Ozone, Aerosol and Radiation (TOAR) [see More Information on ACP Special Issue, available at: http://www.atmos-chem-phys.net/special_issue331.html], vertical profiles of aerosols over the southeastern Tibetan Plateau were measured in June and July of 2014. In this paper, we present the results from balloon borne radiosonde measurements, and investigate the effect of hygroscopic growth on the observed sizes and optical properties of fine particles in the UTLS over the Tibetan Plateau.

2. Experiment

The field experiment was carried out at the Linzhi Meteorological Bureau (29.67°

N, 94.33º E; 2992 m above sea level), located in the southeastern Tibetan Plateau, from June 6 to July 31, 2014. During the field campaign, seven balloon sondes were launched, with each sounding taking place at about 16:00 UTC on June 18 (case 1), June 24 (case 2), July 6 (case 3), July 15 (case 4), July 21 (case 5), July 25 (case 6) and July 30 (case 7), respectively. The balloon sonde payload was composed of a Compact Optical Backscatter AerosoL Detector (COBALD) instrument, iMet and RS92 radiosondes, and a cryogenic frost-point hygrometer (CFH). The payload was lifted by a 1600 g latex balloon, which ascended at a rate of 5-7 m s^{-1}. Data were obtained from the lunching point until an altitude between 30 km to 35 km where the balloon generally burst. In this study, only the ascent data are analyzed.

2.1 COBALD particle backscatter sonde

The lightweight COBALD, developed by Prof. Thomas Peter's group at ETH Zurich, uses two high power light emitting diodes (LEDs) operating at 455nm (blue) and 940nm (infrared) with a silicon detector averaging the light scattered back from molecules or aerosols at angles centered near 173º for typically one-second time periods [Rosen and Kjome, 1991; Wienhold, 2012; Cirisan et al., 2014]. COBALD measurements are only carried out at local nighttime as daylight saturates the sensitive detector. Before flight, the signal from each backscatter sonde is compared with a dedicated set of four standard backscatter sondes maintained in Laramie. The repeatability of the relative calibration between backscatter sondes is about ±1%. The absolute calibration is believed accurate to better than ±3%. Since naturally occurring aerosol backscatter ratios may be quite low, especially in the blue channel, it is important to consider potential sources of error and uncertainty in the absolute values derived from the basic measurements themselves. In the blue channel, a conservative adjustment procedure has been made in the range of 0 to 4% to eliminate nonphysical average values occurring in the troposphere [Rosen et al., 1997].

Backscatter ratios (BSR) at two wavelengths are retrieved from COBALD measurement, which is defined as,

$$BSR = \frac{\beta_a + \beta_m}{\beta_m} = \frac{N_a \cdot \sigma_a + N_m \cdot \sigma_m}{N_m \cdot \sigma_m} \qquad (1)$$

where β denotes backscatter coefficient, N the number concentration, and σ the backscatter cross section. The subscripts a and m indicate contributions from aerosol particles and air molecules, respectively. The backscatter cross section for air molecules can be calculated from Rayleigh scattering theory and the number concentration for air molecules is derived from atmospheric pressure and temperature measured by the radiosonde. The backscattering cross section for aerosol particles can be calculated from Mie scattering theory for a specified effective radius. The aerosol backscatter ratio (ABSR) is defined as,

$$ABSR = \frac{\beta_a}{\beta_m} = BSR - 1 \qquad (2)$$

The ABSR values at two wavelengths are used to calculate the Color Index [CI, Rosen et al., 1997], which is defined as the ABSR at 940 nm divided by the ABSR at 455 nm. The CI is proportional to the ratio of the backscatter cross sections at 940 and 455 nm, and hence it can provide an estimate of the particle size. Assuming an index of refraction of 1.45 with 75% sulfate and a typical lognormal size distribution of the stratospheric aerosols [Rosen and Kjome, 1991], the backscatter cross sections σ_a at the wavelengths used by COBALD are calculated by Mie theory, and further the CI as a function of the mean radius of total aerosol particles is derived. Because no information on standard deviation of the lognormal distribution is available, the possible lower and upper limits of the standard deviation are assumed to be 1.8 and 2.2 [Deshler et al., 2003]. By comparing the observed CI with the calculated one for different standard deviations, the range of possible mean radius can be obtained, and the number concentration and further volume concentration for aerosol particles can be retrieved from the observed ABSR according to the Equation (1).

2.2 Radiosonde observations

In this study we use the air temperature profiles from the RS92 radiosondes with an uncertainty of $\pm 0.2°C$ below 100 hPa and $\pm 0.3°C$ between 100 and 20 hPa. The profiles of water vapor are obtained from CFH measurements. The CFH is a microprocessor-controlled instrument with a lightweight of 400 g, and it uses a cryogenic liquid as cooling agent and operates based on the chilled-mirror principle

[Vömel et al., 2007a]. The uncertainty of frost point or dew point measured by the CFH is smaller than 0.2 K. Correspondingly, the uncertainty in relative humidity is estimated to be 2 % for measurement in the lower troposphere and 5 % in the tropical tropopause region [Vömel et al., 2016]. As a standard for water vapor measurements, CFH has been used in numerous intercomparison experiments, such as the validation of Aura Microwave Limb Sounder (MLS) water vapor products, globally [Vömel et al., 2007b] and specifically over the Tibetan Plateau [Yan et al., 2016].

3. Results and discussion

Figure 1 shows the BSR profiles at two wavelengths and calculated CI profiles from COBALD measurement, as well as the profiles of temperature and RH over ice respectively from RS92 and CFH measurement for three typical cases on June 18, July 15 and 25, 2014. The COBALD measurements suggest an enhanced aerosol layer (BSR (455 nm)>1.1 and BSR (940 nm)>1.4) extending from 200 hPa (~12 km) to 10hPa (~28 km) with a maximum above the tropopause (90 hPa, ~17 km). The enhanced aerosol layer from COBALD measurement is a mixture of ATAL and the on-setting Junge Layer due to the signal above 50 hPa stemming from the Junge Layer but the maximum occurring in ATAL. The RHi near the maximum of the enhanced aerosol layer varies from 30% to 40%, indicating that it is impossibly caused by cirrus cloud, which cannot persist at these dry conditions. The calculated CI of the enhanced aerosol layer is around 5 (4−8), far below CI of cirrus cloud (being around 10 with the maximum value exceeding 20) at 250 hPa [Vernier et al., 2015].

On February 13, 2014 the Mt. Kelud (8°S, 112°E) in Indonesia erupted, with a volcanic plume located near 18-21 km within the tropical stratosphere, which was detected 11 days after the eruption by the Cloud-Aerosol Lidar with Orthogonal Polarization (CALIOP) onboard the Cloud-Aerosol Lidar and Infrared Pathfinder Satellite Observation (CALIPSO) [Vernier et al, 2016]. Stratospheric aerosols were perturbed significantly by the Kelud volcanic plumes, especially the fresh ash plume in the southern hemisphere [Vernier et al, 2016; Sakai et al., 2016]. The Kelud volcanic eruption might have negligible influence on the observed aerosols in the ATAL, since

the ATAL began to form about four months after the Kelud eruption when the volcanic materials in the troposphere might have vanished. On the other hand, CALIOP data analysis also showed that sulfate components from the Kelud volcanic eruption, peaking at an higher altitude with a longer residence time compared with the volcanic ashes, influenced aerosol optical depth (AOD) between 20°N and 20°S 18-25 km considerably three months after the eruption [Vernier et al, 2016]. It is likely that sulfate aerosols from the Kelud eruption contributed to stratospheric background aerosols above the ATAL and even in the Junge layer at slightly higher latitude, as indicated by our COBALD measurements.

Pinnick et al. [1975] adopted a lognormal distribution with a mode radius of 0.0725 µm and standard deviation (σ) of 1.86 to parameterize the background aerosols in the stratosphere. Rosen and Kjome [1991] suggested a mode radius between 0.04 and 0.06 µm and σ value of ~2.0-2.2 for the 20-km stratospheric aerosol background layer. In this study, the CI as a function of mode radius was derived from Mie calculation using a lognormal distribution for different size of aerosols with standard deviations (σ) of 1.8 and 2.2 respectively and the result is shown in Fig. 2. The signal to noise ratio at the blue channel with respect to the molecular Rayleigh backscatter at tropopause conditions (taken 100 hPa and 210 K) is 220. Given the molecular backscatter coefficient of $4.4e^{-7}$ ($sr^{-1}m^{-1}$) for 455 nm, this corresponds to a backscatter coefficient minimum detection limit of $2e^{-9}$ ($sr^{-1}m^{-1}$), which is holding in general over the entire profile. To define an aerosol size limit, typical aerosol dumber densities need to be assumed: $10\,cm^{-3}$ for stratospheric background and $100\,cm^{-3}$ for the ATAL. The aerosol backscatter coefficients of different aerosol mode radius for the typical aerosol dumber densities are calculated by Mie theory and listed in Table 1. The results confirm that the particles with 100 nm radius are well detected under background conditions, which mainly contribute to the particulate backscatter ratio of approx. 0.01 and is always present. With increasing particle number density, the particles with 30 nm radius start to contribute to the particulate backscatter ratio (> $2e^{-9}$ $sr^{-1}m^{-1}$). Therefore, the lower size boundary that cannot be observed by COBALD due to the lack of scattering efficiency of small aerosols can be defined as 30 nm.

The CI increases monotonously from 1 to 15 with mode radius growing from 1 nm to 1μm. The CI of the enhanced aerosol layer from COBALD measurement usually varied from 4 to 8 as indicated in this figure. With the assumed lognormal widths, the measured CI imposes an upper limit of 100 nm on the particle radius. Therefore, we conclude that the enhanced aerosol layer is composed of a large number of fine particles with radius less than 0.1 μm. It has been documented that aerosols in the UTLS are mainly composed of liquid inorganics with typical mode radii smaller than 0.1 μm [Tobo et al., 2007]. Our observations in Linzhi are consistent with previous findings.

The middle troposphere over the Tibetan Plateau is likely to act as a pipe for the transport of water vapor from the marine boundary layer (i.e., Indian Ocean and South China Sea) to the UTLS, leading to an increase of H_2O mixing ratio near the tropopause [Fu et al., 2006; Lelieveld et al., 2007]. Figure 3(a) presents the CFH H_2O profiles from 110 hPa (~16 km ASL) to 90 hPa (~17.5 km ASL). It is noticed that H_2O mixing ratio changes greatly in the vertical direction (3~12ppmv) for some cases. The dehydration process results in minimum H_2O mixing ratio just above the altitude of each lowest temperature. Pronounced decrease of the H_2O mixing ratio from 110 hPa to 90 hPa are attributed to convective transport of moist air parcels just occurring during the balloon flying periods. The three relatively uniform H_2O profiles (on June 18, July 25 & 30) correspond to the well mixed status of strong upward transport prior to the balloon-based measurements. The water vapor cycle driven by synoptic-scale convection increases the possibility of aerosol hygroscopic growth near the tropopause over the Tibetan plateau. It has been estimated that the scattering ratio could increase by 10% to 50% with a water vapor mixing ratio enhancement from 3 ppmv to 6 ppmv [Vernier et al., 2011].

Fig. 3(b) presents the variation of CI with RHi for all cases between 50 hPa and 150 hPa, the typical altitude range for the ATAL. The dependence of CI on RHi can be classified into three types according to the CI of dry aerosols, i.e. the aerosols existing at very low relative humidity (e.g., RHi < 20%):

(1) When the CI of dry aerosol is larger than about 6, CI of the enhanced aerosol layer shows an exponential growth with increasing RHi;

(2) When the CI of dry aerosol is smaller than about 6, CI of the enhanced aerosol layer decreases with increasing RHi in a slope of -0.03;

(3) When the CI of dry aerosol is close to 6, it keeps almost constant with variation of RHi.

As the CI can be regarded as an indicator of aerosol particle size, it can be inferred that for those aerosol particles with large dry sizes (Type 1, i.e., CI> 6), increasing RHi facilitates water vapor and other gaseous precursors to condense onto pre-existing aerosol particles and then contribute to the particle growth. For those with small dry sizes (Type 2 and Type 3, i.e., CI <= 6), the situation appears to be more completed and cannot be fully understood without more detailed information about aerosol chemical composition and their gas precursors. Since all these aerosol particles were observed at very low RHi, well below 40% deliquescence relative humidity of most of the salts (e.g., 40% for NH_4HSO_4) [Benson et al., 2009], the hygroscopic growth should have negligible effect on the size of these particles under this condition. New particle formation through the gas-to-particle conversion process, which tends to become faster with increasing RH [Fountoukis and Nenes, 2007], increases the number concentration, resulting in decrease of mode radius of bulk aerosols. Therefore, the decrease of CI with RHi (Type 2) indicates that new particle formation might play an important role in the formation and prevalence of fine particles in the UTLS over the Tibetan Plateau.

Based on the BSR and CI at the UTLS altitudes (50-150 hPa) from COBALD, we calculated the aerosol volume concentration in the enhanced aerosol layer for the two typical CI variation trend according to an assumption of lognormal size distribution with standard deviation of 1.8. The variation of aerosol volume concentration distributions with RHi is shown in Fig. 4. It can be seen from Fig 4a that when RHi is less than 60%, aerosol mode radius ranges mostly between 0.04 and 0.07 μm, and it increases steeply to 0.2 μm when RHi is more than 60%. The aerosol volume concentrations are obviously high compared with those in dry condition, especially for those particles with a mode radius of 0.1 μm. For those aerosols with small initial dry particle size (as shown in Fig 4b), accompanied by a mode radius decrease from 0.04 to 0.03 μm, the aerosol volume concentration increases by 4-5 times when RHi rises

from nearly zero to 40%, indicating that the number concentrations experience an explosive increase due to the formation of new particles.

4. Conclusions

The vertical profiles of aerosol BSR measured over the southeastern Tibetan Plateau during summertime demonstrate an enhanced aerosol layer, consisting predominantly of fine particles with mode radius smaller than 0.1 μm, in the UTLS. The size of particles in the enhanced aerosol layer shows an exponential increase with increasing RHi when the CI of dry aerosols is larger than 6 (corresponding mode radius larger than 0.04 μm). It can be inferred that increasing RHi leads to more condensation of water vapor onto pre-existing aerosol particles and contributes to the particle growth. For the CI of dry aerosols smaller than about 6 (i.e., mode radius smaller than 0.04 μm), the size of particles in the enhanced aerosol layer decreases with increasing RHi when RHi is below 40%, lower than typical aerosol deliquescence point. In this case, new particle formation, which results in a decrease of aerosol mode radius and an increase of number concentration, can play an important role in the accumulation of large amounts of fine particles in the UTLS over the Tibetan Plateau. It must be borne in mind that the conclusions drawn from this study are only based on 7 balloon flights so that general conclusions should be established with caution. In fact, chemical interactions involved in the stratosphere troposphere exchange are complicated and further experimental and model studies are needed to understand the nature and origin of the ATAL and its influence on global atmospheric chemistry and climate.

Author Contributions

Qianshan He, Jianzhong Ma and Xiangdong Zheng designed the study. Holger Vömel and Frank G. Wienhold respectively contributed to data quality control of COBALD and CFH. Guangming Shi calculated Mie scattering parameters. Wei Gao, Dongwei Liu and Tiantao Cheng contributed to data analysis, numerical experiments, interpretation and paper writing. Xiaolu Yan executed the in-situ balloon sondes observation. Qianshan He did further analysis and interpreted the results. All authors

contributed to improve the manuscript.

Acknowledgements. This study was supported by the National Natural Science Foundation of China (Grant No. 91637101, 91837311 and 91537213) and the Shanghai Science and Technology Committee Research Project (Grant No. 16ZR1431700). We thank all TOAR team members and the staff from the Tibet Meteorological Service for assisting our experiment work. We also thank Dr. Yutaka Tobo, whose useful suggestions have greatly improved the paper.

References

Benson, D. R., Erupe, M. E., and Lee, S. H.: Laboratory-measured H_2SO_4-H_2O-NH_3 ternary homogeneous nucleation rates: Initial observations, Geophys. Res. Lett., 36, 10.1029/2009gl038728, 2009.

Bian, J., Pan, L. L., Paulik, L., Vmel, H., Chen, H., and Lu, D.: In situ water vapor and ozone measurements in Lhasa and Kunming during the Asian summer monsoon, Geophys. Res. Lett., 39(19), 19808, 2012.

Carslaw, K. S., Luo, B. P., Clegg, S. L., Peter, T. H., Brimblecombe, P., and Crutzen, P. J.: Stratospheric aerosol growth and HNO_3 gas phase depletion from coupled HNO3 and water uptake by liquid particles, Geophys. Res. Lett., 21, 2479–2482, 1994.

Cirisan, A., Luo, B. P., Engel, I., Wienhold, F. G., Krieger, U. K., Weers1, U., Romanens, G., Levrat, G., Jeannet, P., Ruffieux, D., Philipona, R., Calpini, B., Spichtinger, P., and Peter, T.: Balloon-borne match measurements of mid-latitude cirrus clouds, Atmos. Chem. Phys., 14, 7341–7365, 2014.

Deshler, T., Hervig, M. E., Hofmann, D. J., Rosen, J. M., and Liley, J. B.: Thirty years of in situ stratospheric aerosol size distribution measurements from Laramie, Wyoming (41N), using balloon-borne instruments, J. Geophys. Res., 108, doi:10.1029/2002JD002514, 2003.

Engel, I.: The Role of Heterogeneous Nucleation in Polar Stratospheric Cloud

Formation: Microphysical Modeling, ETH ZURICH, Doctor Dissertation, 2013.

English J. M., Toon, O. B., Mills, M. J., and Yu, F.: Microphysical simulations of new particle formation in the upper troposphere and lower stratosphere, Atmos. Chem. Phys., 11, 9303–9322, 2011.

Fadnavis, S., Semeniuk, K., Pozzoli, L., Schultz, M. G., Ghude, S. D., Das, S., and Kakatkar, R.: Transport of aerosols into the UTLS and their impact on the Asian monsoon region as seen in a global model simulation, Atmos. Chem. Phys., 13(17), 8771-8786, 2013.

Fountoukis, C., and Nenes, A.: ISORROPIA II: a computationally efficient thermodynamic equilibrium model for K^+ -Ca^{2+} -Mg^{2+} -NH^{4+} -Na^+ -SO_4^{2-} -NO^{3-} -Cl^- -H_2O aerosols, Atmos. Chem. Phys., 7, 4639-4659, 10.5194/acp-7-4639-2007, 2007.

Fu, R., Hu, Y., Wright, J. S., Jiang, J. H., Dickinson, R. E., Chen, M., Filipiak, M., Read, W. G., Waters, J. W., and Wu, D. L.: Short circuit of water vapor and polluted air to the global stratosphere by convective transport over the Tibetan Plateau, Proc. Natl. Acad. Sci. U. S. A., 103, 5664–5669, doi:10.1073/pnas.0601584103, 2006.

Gettelman, A., Hoor, P., Pan, L. L., Randel, W. J., Hegglin, M. I., and Birner, T.: The extratropical upper troposphere and lower stratosphere, Rev. Geophys., 49(3), RG3003, 2011.

He, Q. S., Li, C. C., Ma, J. Z., Wang, H. Q., Yan, X. L., Lu, J., Liang, Z. R., and Qi, G. M.: Lidar-observed enhancement of aerosols in the upper troposphere and lower stratosphere over the Tibetan Plateau induced by the Nabro volcano eruption, Atmos. Chem. Phys., 14, 1-9, 2014.

Kim, Y. S., Shibata, T., Iwasaka, Y., Shi, G. Y., Zhou, X. J., Tamura, K., and Ohashi, T.: Enhancements of aerosols near the cold tropopause in summer over Tibetan Plateau: Lidar and balloon borne measurements in 1999 at Lhasa, Tibet, China. Proc SPIE, 4893, 496-503, doi:10.1117/12.466090, 2003.

Lelieveld, J., Brühl, C., Jackel, P., Steil, B., Crutzen, P. J., Fischer, H., Giorgetta, M. A., Hoor, P., Lawrence, M. G., Sausen, R., and Tost, H.: Stratospheric dryness: model simulations and satellite observations, Atmos. Chem. Phys., 7, 1313-1332,

doi:10.5194/acp-7-1313-2007, 2007.

Li, Q.: Trapping of Asian pollution by the Tibetan anticyclone: A global CTM simulation compared with EOS MLS observations, Geophys. Res. Lett., 32, L14826, doi:10.1029/2005GL022762, 2005.

Martinsson, B. G., Friberg, J., Andersson, S. M., Weigelt, A., Hermann, M., Assmann, D., Voigtländer, B. C. A. M., van Velthoven, P. J. F., and Zahn, A.: Comparison between CARIBIC aerosol samples analyzed by accelerator-based methods and optical particle counter measurements, Atmos. Meas. Tech., 7, 2581–2596, doi:10.5194/amt-7-2581-2014, 2014.

Li, D., Vogel, B., Bian, J., Müller, R., Pan, L. L., Günther, G., Bai, Z., Li, Q., Zhang, J., Fan, Q., and Vömel, H.: Impact of typhoons on the composition of the upper troposphere within the Asian summer monsoon anticyclone: the SWOP campaign in Lhasa 2013, Atmos. Chem. Phys., 17, 4657-4672, 10.5194/acp-17-4657-2017, 2017.

Park, M., Randel, W. J., Kinnison, D. E., Garcia, R. R., and Choi, W.: Seasonal variation of methane, water vapor, and nitrogen oxides near the tropopause: Satellite observations and model simulations, J. Geophys. Res., 109, D03302, doi:10.1029/2003JD003706, 2004.

Park, M., Randel, W. J., Gettelman, A., Massie, S. T., and Jiang, J. H.: Transport above the Asian summer monsoon anticyclone inferred from Aura Microwave Limb Sounder tracers, J. Geophys. Res., 112, D16309, doi:10.1029/2006jd008294, 2007.

Pierce, J. R., and Adams, P. J.: Can cosmic rays affect cloud condensation nuclei by altering new particle formation rates? Geophys. Res. Lett., 36, L09820, doi:10.1029/2009GL037946, 2009.

Pinnick, R. G., Rosen, J. M., and Hofmann, D. J.: Stratospheric Aerosol Measurements III: Optical Model Calculations, J. Atmos. Sci., 33, 304-314, 1975.

Randel, W. J., Park, M., Emmons, L., and Pumphrey, H. C.: Asian monsoon transport of pollution to the stratosphere, Science, 328, 611-613, doi:10.1126/science.1182274, 2010.

Rosen, J., and Kjome, N.: Backscatter sonde: a new instrument for atmospheric aerosol research, Appl. Opt., 30, 1552–1561, 1991.

Rosen, J., Kjome, N., and Liley, J.: Tropospheric aerosol backscatter at a midlatitude site in the northern and southern hemispheres, J. Geophys. Res., 102, D17, 21329-21339, 1997.

Sakai, T., Uchino, O., Nagai, T., Liley, B., Morino, I., and Fujimoto, T.: Long-term variation of stratospheric aerosols observed with lidars over tsukuba, japan, from 1982 and lauder, new zealand, from 1992 to 2015, J. Geophys. Res., 121(17), 10283-10293, 2016.

Solomon, S., Daniel, J. S., Neely III, R. R., Vernier, J. P., Dutton, E. G., and Thomason, L. W.: The persistently variable background stratospheric aerosol layer and global climate change, Science, 333, 866-870, doi:10.1126/science.1206027, 2011.

Schlager, H., and Arnold, F.: Measurement of stratospheric gaseous nitric acid in the Winter arctic vortex using a novel rocket-borne mass spectrometer method, Geophys. Res. Lett., 17, 433–436, 1990.

Tabazadeh, A., Turco, R. P., and Jacobson, M. Z.: A model for studying the composition and chemical effects of stratospheric aerosols, J. Geophys. Res., 99, 12897-12914, 1994.

Thomason, L. W., and Vernier, J. P.: Improved SAGE II cloud/aerosol categorization and observations of the Asian tropopause aerosol layer: 1989-2005, Atmos. Chem. Phys., 13, 4605-4616, doi:10.5194/acp-13-4605-2013, 2013.

Timmreck, C., Graf, H. F., Lorenz, S. J., Niemeier, U., Zanchettin, D., Matei, D., Jungclaus, J. H., and Crowley, T. J.: Aerosol size confines climate response to volcanic super-eruptions, Geophys. Res. Lett., 37, L24705, doi:10.1029/2010GL045464, 2010.

Tobo, Y., Iwasaka, Y., Shi, G. Y., Kim, S., Ohashi, T., Tamura, K., and Zhang, D. Z.: Balloon-borne observations of high aerosol concentrations near the summertime tropopause over the Tibetan Plateau, Atmos. Res., 84, 233-241, doi: 10.1016/j.atmosres.2006.08.003, 2007.

Vernier, J. P., Thomason, L. W., and Kar, J.: CALIPSO detection of an Asian tropopause

aerosol layer, Geophys. Res. Lett., 38, L07804, doi:10.1029/2010GL046614, 2011.

Vernier, J. P., Fairlie, T. D., Natarajan, M., Wienhold, F. G., Bian, J., Martinsson, B. G., Crumeyrolle, S., Thomason, L. W., and Bedka, K. M.: Increase in upper tropospheric and lower stratospheric aerosol levels and its potential connection with Asian pollution, J. Geophys. Res. Atmos., 120, 1608–1619, , 2015.

Vernier, J. P., Fairlie, T. D., Deshler, T., Natarajan, M., Knepp, T., and Foster, K.: In situ and space‐based observations of the kelud volcanic plume: the persistence of ash in the lower stratosphere, J. Geophys. Res. Atmos., 121(18), 11104-11118, 2016.

Vernier, J. P., Fairlie, T. D., Deshler, T., Kumar, B. S., Natarajan, M., Pandit, A. K., Akhil Raj, S. T., Hemanth Kumar, A., Jayaraman, A., Singh, A., Rastogi, N., Sinha,P. R., Kumar, S., Tiwari, S., Wegner, T., Baker, N., Vignelles, D., Stenchikov, G., Shevchenko, I., Smith, J., Bedka, K., Kesarkar, A., Singh, V., Bhate, J., Ravikiran, V., Durga Rao, M., Ravindrababu, S., Patel, A., Vernier, H., Wienhold, F. G., Liu, H., Knepp, T. N., Thomason, L., Crawford, J., Ziemba, L., Moore, J., Crumeyrolle, S., Williamson, M., Berthet, G., Jégou, F., and Renard, J. B.: BATAL: The Balloon measurement campaigns of the Asian Tropopause Aerosol Layer. Bulletin of the American Meteorological Society, BAMS-D-17-0014.1, 2017.

Voigt, C., Schlager, H., Roiger, A., Stenke, A., de Reus, M., Borrmann, S., Jensen, E., Schiller, C., Konopka, P., and Sitnikov, N.: Detection of reactive nitrogen containing particles in the tropopause region – evidence for a tropical nitric acid trihydrate (NAT) belt, Atmos. Chem. Phys., 8(24), 7421-7430, doi:10.5194/acp-8-7421-2008, 2008.

Vömel, H., Selkirk, L., Miloshevich, J., Valverde-Canossa, J., Valdes, J., and Diaz, J.: Radiation Dry Bias of the Vaisala RS92 Humidity Sensor, J. Atmos. Ocean. Tech., 24, 953–963, 2007a.

Vömel, H., Barnes, J. E., Forno, R., Fujiwara, M., Hasebe, F., Iwasaki, S., Kivi, R., Komala, N., Kyrö, E., Leblanc, T., Morel, B., Ogino, S. Y., Read, W. G., Ryan, S.

C., Saraspriya, S., Selkirk, H., Shiotani, M., Valverde Canossa, J., and Whiteman, D. N.: Validation of Aura Microwave Limb Sounder water vapor by balloon-borne Cryogenic Frost point Hygrometer measurements, J. Geophys. Res., 112(D24), doi:10.1029/2007JD008698, 2007b.

Vömel, H., Naebert, T., Dirksen, R., and Sommer, M.: An update on the uncertainties of water vapor measurements using cryogenic frost point hygrometers, Atmos. Meas. Tech., 9, 3755-3768, doi:10.5194/amt-9-3755-2016, 2016.

Weigel, R., Borrmann, S., Kazil, J., Minikin, A., Stohl, A., Wilson, J. C., Reeves, J. M., Kunkel, D., de Reus, M., Frey, W., Lovejoy, E. R., Volk, C. M., Viciani, S., D'Amato, F., Schiller, C., Peter, T., Schlager, H., Cairo, F., Law, K. S., Shur, G. N., Belyaev, G. V., and Curtius, J.: In-situ observations of new particle formation in the tropical upper troposphere: The role of clouds and the nucleation mechanism, Atmos. Chem. Phys., 11, 9983–10010, doi:10.5194/acp-11-9983-2011, 2011.

Wienhold, F. G.: http://www.iac.ethz.ch/groups/peter/research/Balloon_soundings/COBALD_sensor, COBALD Data Sheet, 2012.

Yan X. L., Wright, J. S., Zheng, X. D., Livesey, N., Vömel, H., and Zhou, X. J.: Validation of Aura MLS retrievals of temperature, water vapour and ozone in the upper troposphere and lower–middle stratosphere over the Tibetan Plateau during boreal summer, Atmos. Meas. Tech., 9, 3547-3566, doi:10.5194/amt-9-3547-2016, 2016.

Yu P., Rosenlof, K. H., Liu, S., Telg, H., and Gao, R. S.: Efficient transport of tropospheric aerosol into the stratosphere via the Asian summer monsoon anticyclone. Proc. Nation. Acad. Sci., 114(27): 6972-6977, 2017.

Table 1 The aerosol backscatter coefficients of different aerosol mode radius for the typical aerosol dumber densities.

Mode Radius (nm)	10	30	100
β_a@10 cm^{-3} (sr^{-1} m^{-1})	1e^{-12}	3e^{-10}	2e^{-8}
β_a@100 cm^{-3} (sr^{-1} m^{-1})	1e^{-11}	3e^{-9}	2e^{-7}
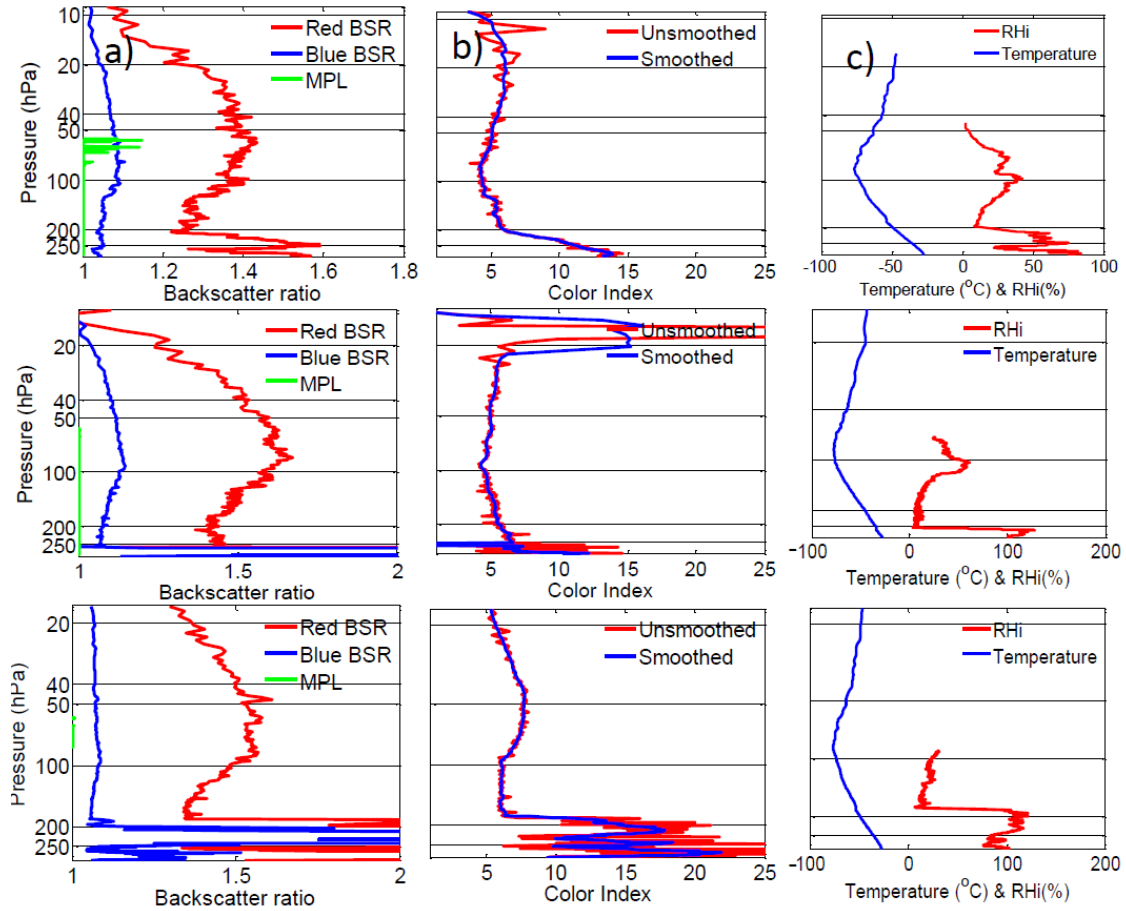
Fig. 1. (a) Three cases of the backscattering ratio profile from COBALD and MPL measurements on June 18 (top), July 15 (middle) and July 25 (bottom), 2014. (b) The calculated CI profiles from the ABSR at two wavelengths. (c) Temperature and RHi profiles measured by the RS92 radiosonde and CFH, respectively.
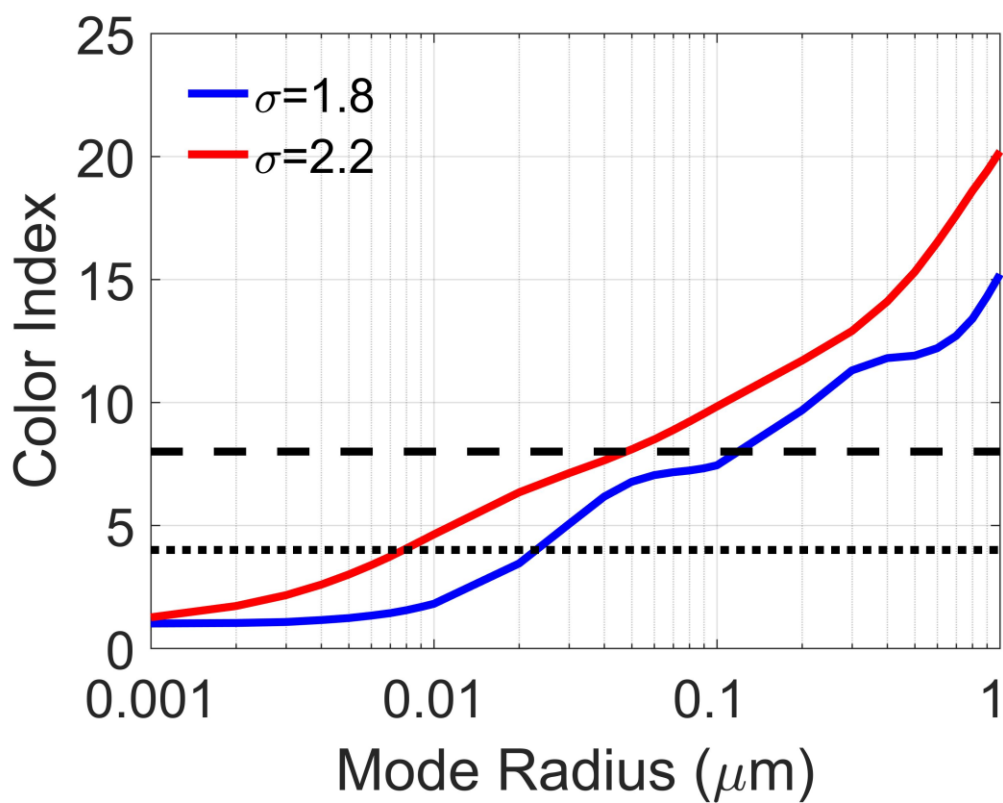
Fig. 2. CI as a function of mode radius from Mie calculation assuming an index of refraction of 1.45 and a lognormal size distribution with the indicated standard deviations (σ) of 1.8 and 2.2. The dotted and dashed lines represent the minimum (~4) and maximum (~8) CI of the enhanced aerosol layer from COBALD measurement for all cases.
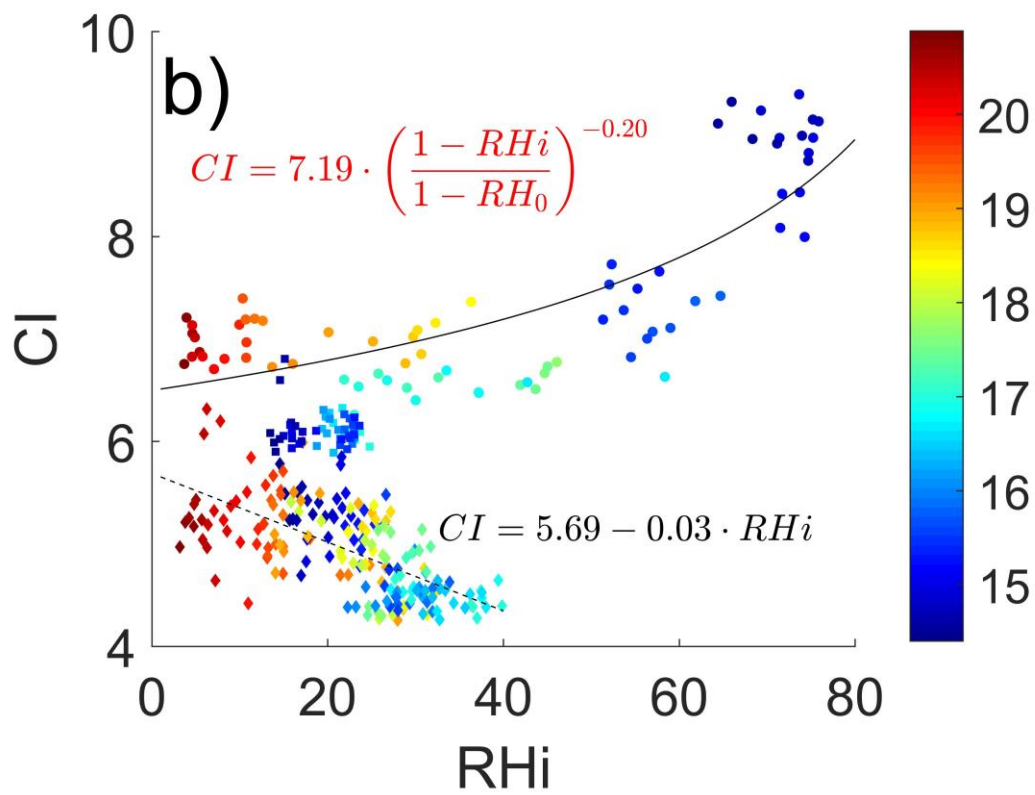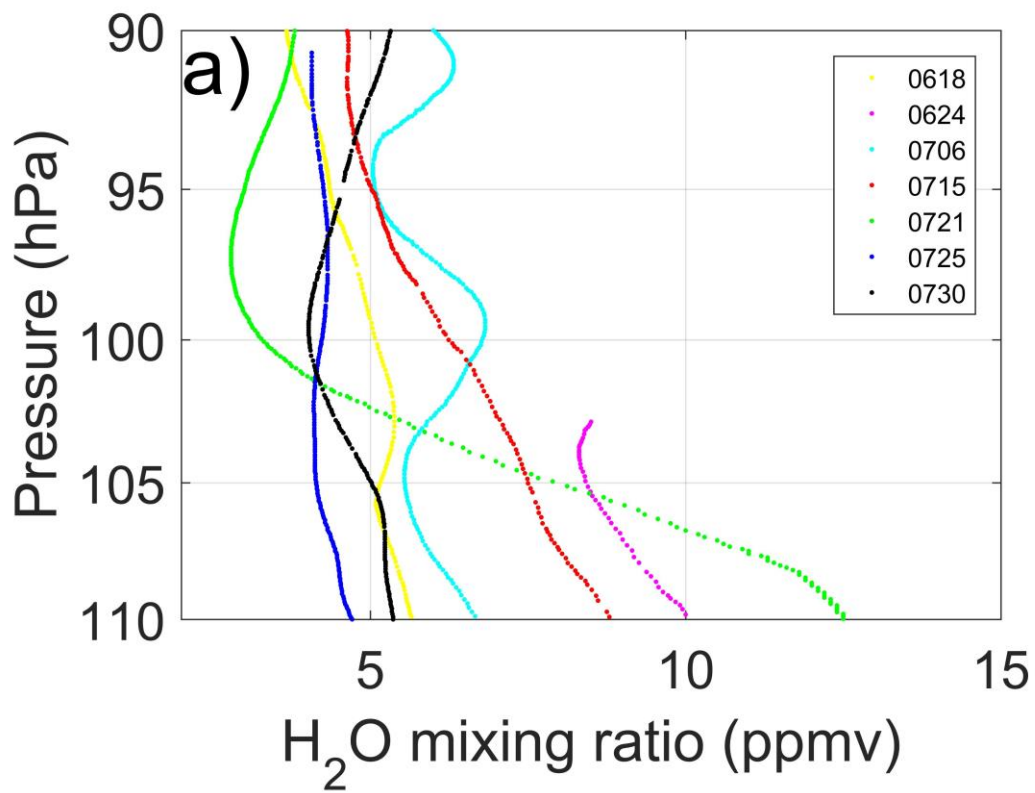
Fig. 3. (a) H$_2$O mixing ratio from CFH measurements, and (b) the variation of CI with

RHi between 50 hPa and 150 hPa for all cases. The circle, square and diamond symbols

refer to those particles with CI of dry aerosol larger than, close to and t smaller than about 6, respectively. The altitude (in unit of km), where particles were measured, is marked with different color. The two fitted equations exceed the 99% significance level.
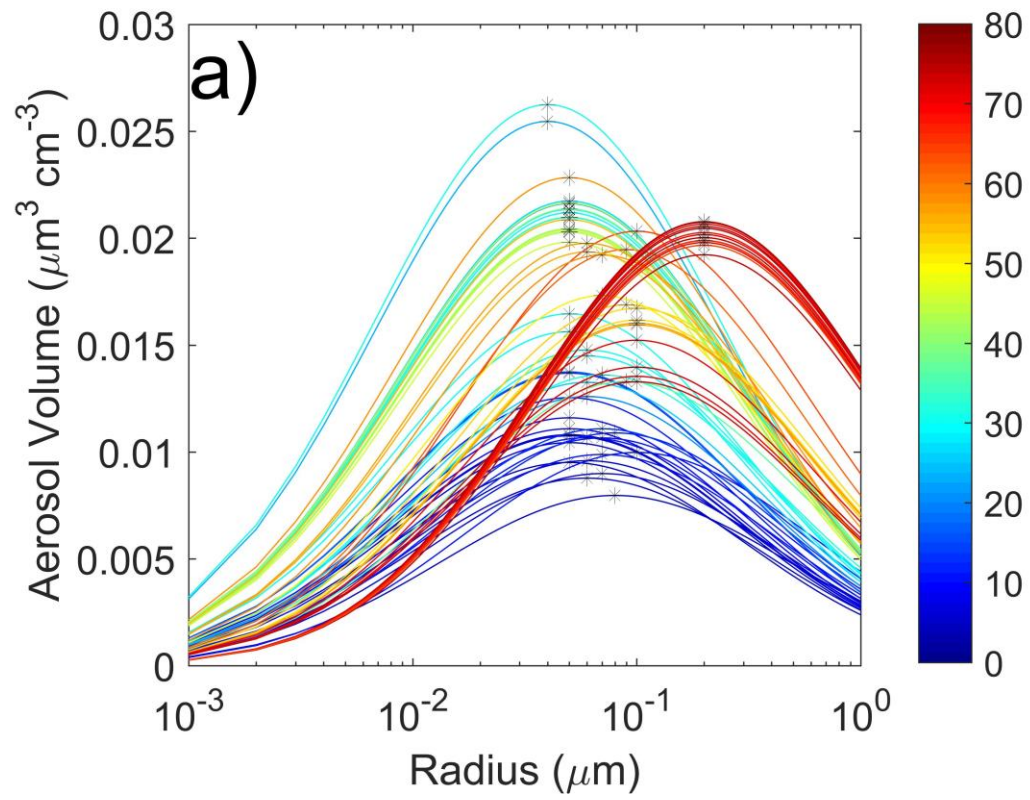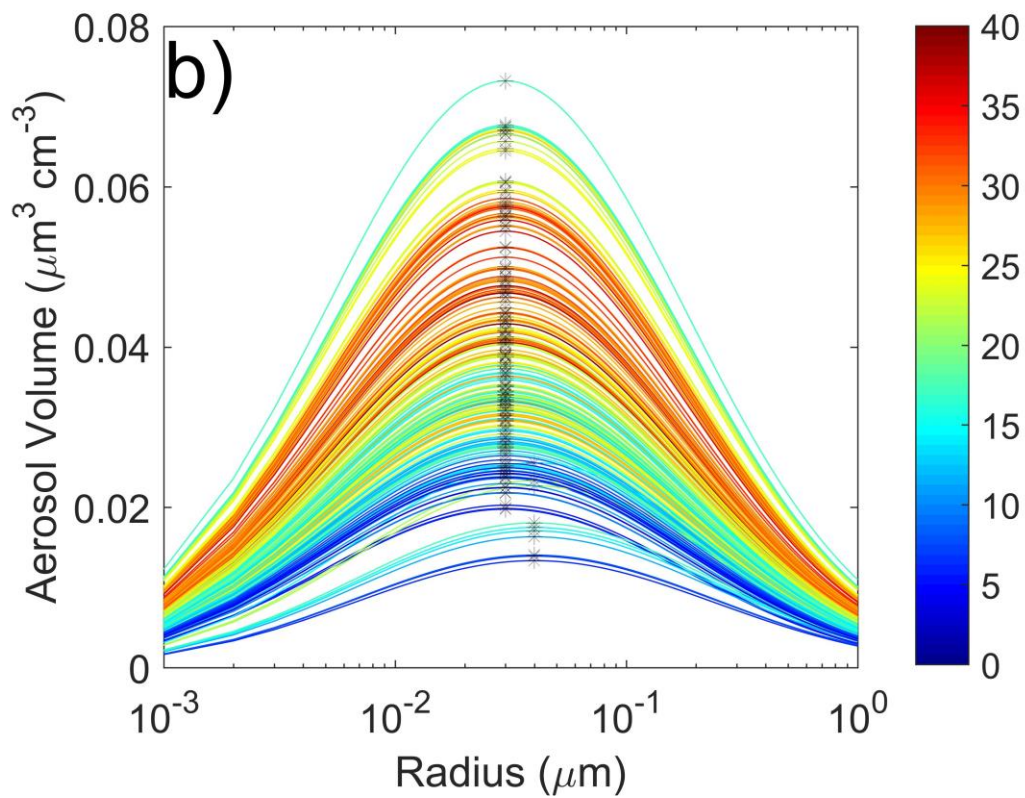
Fig. 4. The variation of aerosol volume concentration distributions in the enhanced aerosol layer with RHi for (a) case 5 (July 21), and (b) the other cases corresponding to the CI<6 case (diamonds) in Fig 3b. The color of each distribution represents RHi labeled on the color bar. The asterisk is mode radius of each distribution.